

CrossMark
click for updatesCite this: *CrystEngComm*, 2015, 17, 1336

Secondary organic moiety templated organic–inorganic polyoxometalate-based frameworks†

Li-Na Xiao,^{ac} La-Mei Wang,^a Xiao-Nan Shan,^b Hai-Yang Guo,^a Li-Wei Fu,^a Yang-Yang Hu,^a Xiao-Bing Cui,^{*a} Ke-Chang Li^{*a} and Ji-Qing Xu^a

Four new organic–inorganic hybrid compounds, namely, $[\text{Cu}_3(4,4'\text{-bpy})_3][\text{HSiW}_{12}\text{O}_{40}] \cdot (\text{C}_3\text{H}_4\text{N}_2)$ (**1**), $[\text{Cu}_3(4,4'\text{-bpy})_3][\text{PMo}_{12}\text{O}_{40}] \cdot (\text{C}_5\text{H}_6\text{N}_2) \cdot 0.5\text{H}_2\text{O}$ (**2**), $[\text{Cu}_2(4,4'\text{-bpy})_2][\text{HPMo}_{12}\text{O}_{40}] \cdot (\text{C}_5\text{H}_6\text{N}_2)$ (**3**) and $[\text{Cu}(\text{Phen})(4,4'\text{-bpy})(\text{H}_2\text{O})_2][\text{PW}_{12}\text{O}_{40}] \cdot (4,4'\text{-bpy})$ (**4**) ($\text{C}_3\text{H}_4\text{N}_2 = \text{imidazole}$, $\text{C}_5\text{H}_6\text{N}_2 = 2\text{-aminopyridine}$, $\text{bpy} = \text{bipyridine}$, $\text{Phen} = 1,10\text{-phenanthroline}$), have been synthesized and characterized by IR, UV-vis, powder XRD, cyclic voltammetry analysis, photoluminescence analysis, elemental analyses and single crystal X-ray diffraction. The four compounds represent new examples of secondary organic moiety templated frameworks constructed from Keggin polyanions, metal ions and organic ligands. Compounds **1** and **2** present 3-D framework structures; compound **3** exhibits a 1-D ladder-like structure and compound **4** shows a 2-D layered framework structure. It is noted that the packing structures of compounds **1** and **2** are almost identical; however, the crystal space groups and cell parameters of the two are thoroughly different. Such a phenomenon has also been observed between compound **3** and a compound recently reported by us. Compound **4** is the first framework structure constructed from polyoxometalates, metal ions and mixed organic ligands. In addition, all the four frameworks are combined with dissociated organic moieties as templates.

Received 10th October 2014,
Accepted 15th December 2014

DOI: 10.1039/c4ce02043j

www.rsc.org/crystengcomm

Introduction

It has been widely recognized that polyoxometalates (POMs) exhibit a variety of structures and properties that make them useful in catalysis, material science and medicine.¹ This class of metal–oxygen clusters is formed by early transition metals of groups V and VI (V, Nb, Ta, Mo and W) in their highest oxidation states (e.g., V^{5+} and W^{6+}). POMs have also been found to be versatile inorganic building blocks for the construction of functional solid materials.² In the past few decades, with the advent of modern high-resolution and sophisticated instrumentation, the number of POM-based functional solid materials has been rising at an exponential rate.³

Recently, a new advance in POM chemistry is that a large number of compounds with 1-D, 2-D and 3-D extended structures constructed from the combination of POMs and transition metal ions or transition metal complexes (TMCs) have been obtained.^{4–9} An intelligent choice of POMs and transition metal ions or TMCs may yield materials with fascinating structures and desirable properties. The diversity of POMs and transition metal ions or TMCs has led to a wide array of functional organic–inorganic hybrid materials. Up to now, most of the existing POMs have already been applied to act as building blocks that can be connected to transition metal ions or TMCs to form extended structures, including Keggin POMs, Dawson POMs and so on.

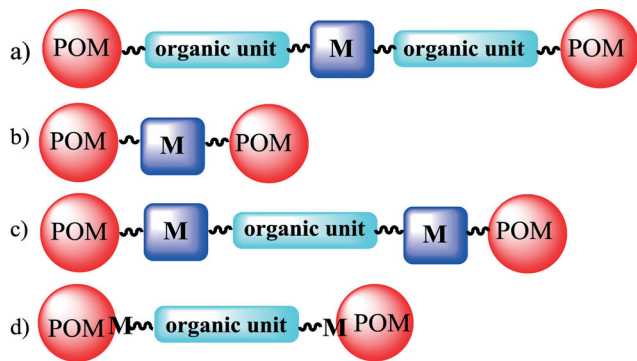
Three main approaches have been developed for the linkage of POMs and transition metal ions or TMCs. The first was represented by $[\text{V}_6\text{O}_{13}\{(\text{OCH}_2)_3\text{C}(\text{NHCH}_2\text{C}_6\text{H}_4\text{-4-CO}_2)\}_2]^{4-}$, in which organic units connect POMs and metal ions to form a novel open framework (Scheme 1(a)).⁴ The second uses dative bonds between POMs and transition metals or between POMs and TMC metals. A large number of such frameworks have been reported,^{5–9} which were directed through interactions between transition metals or TMC metals serving as inorganic bridging linkers and oxygens of POMs (Scheme 1(b)). Recently a new approach has been developed for frameworks based on POMs and transition

^a College of Chemistry and State Key Laboratory of Inorganic Synthesis and Preparative Chemistry, Department of Chemistry, Jilin University, Changchun 130023, China. E-mail: cuixb@mail.jlu.edu.cn

^b State Key Laboratory of Luminescence Applications, Changchun Institute of Optics, Fine Mechanics and Physics, Chinese Academy of Science, Changchun 130033, China

^c Department of Chemistry, Zhoukou Normal University, Henan, Zhoukou 466001, China

† Electronic supplementary information (ESI) available. CCDC 1006424 for **1**, 1006425 for **2**, 1006426 for **3** and 1006427 for **4**. For ESI and crystallographic data in CIF or other electronic format see DOI: 10.1039/c4ce02043j



Scheme 1 Schematic representation of the three major ways to connect POMs in POMMOFs (a–c) and the way to connect substituted POMs in POMOFs (d). M: transition metal ions.

metal ions, in which, besides the interactions between POMs and transition metal ions, a new kind of interactions can occur *via* intermediary bidentate or multidentate organic ligands between or among transition metal ions. That is to say, both transition metal ions and organic ligands in the frameworks act as bridges. Each transition metal acts as a bridge connecting a neighboring POM and a neighboring organic ligand, and simultaneously each organic ligand acts as a bridge joining two neighboring transition metal ions. Thus, through the two types of interactions, a kind of POM-based framework structure built from the connection of saturated POMs, metal ions and organic linkers, so-called POMMOFs, has emerged.¹⁰ It should be noted that POMMOFs exhibit a novel POM–M–L–M–POM linking fashion (Scheme 1(c)). The properties and diverse coordination modes of saturated POMs and metal ions together with the diversity of organic linkers provide an impetus for the synthesis of multifunctional materials.

There also exists a similar kind of POM based framework structure, the so-called POMOFs.¹¹ We have found that most of the POMOFs reported are based on substituted POMs (SPOMs) and organic ligands. The linking fashion of this kind of POM based framework can be regarded as –SPOM–L–SPOM– (Scheme 1(d)), which is thoroughly different from that of POMMOFs.

Inorganic frameworks supported by organic moieties such as zinc phosphates or metal–organic frameworks with guest organic moieties are very important to chemists.¹² POMMOFs are also a framework structure, which should be similar to the abovementioned two and can be templated by the guest; therefore the size and stability of the assembly will be promoted by the complementarity between the host and the guest. If the integrity of the POMMOF framework is retained with guest molecules removed or readsorbed, the framework will be useful in many fields. Therefore, we began to search for organic moiety templated POMMOFs by introducing an extra organic species.

In this manuscript, we report the preparation and characterization of four new secondary organic moiety templated POMMOFs: $[\text{Cu}_3(4,4'\text{-bpy})_3][\text{HSiW}_{12}\text{O}_{40}] \cdot (\text{C}_3\text{H}_4\text{N}_2)$ (1), $[\text{Cu}_3(4,4'\text{-bpy})_3][\text{PMo}_{12}\text{O}_{40}] \cdot (\text{C}_5\text{H}_6\text{N}_2) \cdot 0.5\text{H}_2\text{O}$ (2),

$[\text{Cu}_2(4,4'\text{-bpy})_2][\text{HPMo}_{12}\text{O}_{40}] \cdot (\text{C}_5\text{H}_6\text{N}_2)$ (3) and $[\text{Cu}(\text{Phen})(4,4'\text{-bpy})(\text{H}_2\text{O})_2][\text{PW}_{12}\text{O}_{40}] \cdot (4,4'\text{-bpy})$ (4). Compounds 1, 2 and 3 all contain $\text{Cu}(4,4'\text{-bpy})_n^{n+}$ infinite chains and $[\text{XM}_{12}\text{O}_{40}]^{n-}$ anions (X = Si for 1, X = P for 2 and 3, M = W for 1, M = Mo for 2 and 3). However, the structures of compounds 1, 2 and 3 are thoroughly different. $\text{Cu}(4,4'\text{-bpy})_n^{n+}$ infinite chains and $[\text{XM}_{12}\text{O}_{40}]^{n-}$ anions in compounds 1 and 2 are both connected to form a novel 3-D network structure, and $\text{Cu}(4,4'\text{-bpy})_n^{n+}$ infinite chains and $[\text{XM}_{12}\text{O}_{40}]^{n-}$ anions in compound 3 are linked to form a 1-D ladder-like structure. In contrast, compound 4 exhibits an unprecedented 2-D layered framework structure in which its TMCs are constructed from two different organic ligands. It is noted that the packing structures of compounds 1 and 2 are almost identical; however, the crystal system and cell parameters of the two are thoroughly different. Such a phenomenon has also been observed between compound 3 and a compound recently reported by us. Compound 4 is the first framework structure constructed from polyoxometalates, metal ions and mixed organic ligands.

2. Experimental

2.1. General procedures

All chemicals used were of reagent grade and used without further purification. C, H, N analyses were carried out on a Perkin-Elmer 2400 CHN elemental analyser. Elemental analyses of Si, P, W, Mo and Cu were performed by inductively coupled plasma (ICP) mass spectrometry on a Perkin-Elmer Optima 3300DV ICP spectrometer. Infrared spectra were recorded as KBr pellets on a Perkin-Elmer SPECTRUM ONE FTIR spectrometer. Emission/excitation spectra were recorded on a RF-540 fluorescence spectrophotometer. UV-vis spectra were recorded in dimethyl sulfoxide solution on a Shimadzu UV-3100 spectrophotometer. X-ray diffraction (XRD) patterns were obtained on a Siemens D5005 diffractometer using $\text{Cu K}\alpha$ radiation. Electrochemical measurements were carried out on a CHI 660B electrochemical workstation. The working electrode was a glassy carbon, and the surface of the glassy carbon working electrode was polished with 1 μm alumina and washed with distilled water before each experiment. The counter electrode was a Pt wire and Ag/AgCl serves as the reference electrode. All measurements were made at room temperature of 25 $^\circ\text{C}$.

2.2. Preparation

2.2.1. Preparation of $[\text{Cu}_3(4,4'\text{-bpy})_3][\text{HSiW}_{12}\text{O}_{40}] \cdot (\text{C}_3\text{H}_4\text{N}_2)$ (1). Compound 1 was synthesized hydrothermally from a mixture of $\text{H}_4[\text{SiO}_4(\text{W}_3\text{O}_9)_4] \cdot x\text{H}_2\text{O}$ (FW \approx 2878.17, 0.4 g, 0.14 mmol), $\text{CuCl}_2 \cdot 2\text{H}_2\text{O}$ (0.23 g, 1.33 mmol), $\text{H}_2\text{C}_2\text{O}_4 \cdot 2\text{H}_2\text{O}$ (0.41 g, 3.25 mmol), im (im = imidazole, 0.027 g, 0.4 mmol), 4,4'-bpy (0.101 g, 0.65 mmol) and distilled water (20 ml). The pH of the mixture was necessarily adjusted to 4 with $\text{NH}_3 \cdot \text{H}_2\text{O}$ solution. The mixture was heated under autogenous pressure at 160 $^\circ\text{C}$ for 5 days and then left to cool to room temperature. Dark red block crystals could be isolated in

about 51% yield (based on W). Elemental analyses (%) calcd.: W, 61.24; Si, 0.78; Cu, 5.29; C, 11.00; H, 0.81; N, 3.11. Found: W, 62.08; Si, 0.84; Cu, 5.16; C, 10.11; H, 0.74; N, 2.97. FT-IR (KBr, cm^{-1}): 1614, 1530, 1414, 1322, 1226, 1070, 1012, 967, 914, 785, 532, 377, 325.

2.2.2. Preparation of $[\text{Cu}_3(4,4'\text{-bpy})_3][\text{PMo}_{12}\text{O}_{40}](\text{C}_5\text{H}_6\text{N}_2)\cdot 0.5\text{H}_2\text{O}$ (2). Compound 2 was synthesized hydrothermally from a mixture of $\text{H}_3\text{Mo}_{12}\text{O}_{40}\cdot \text{P}\cdot \text{xH}_2\text{O}$ (FW \approx 1825.25, 0.5 g, 0.274 mmol), NH_4VO_3 (0.234 g, 2.0 mmol), $\text{C}_8\text{H}_6\text{O}_4$ (isophthalic acid) (0.30 g, 1.81 mmol), $\text{CuCl}_2\cdot 2\text{H}_2\text{O}$ (0.333 g, 1.953 mmol), 4,4'-bpy (0.166 g, 0.864 mmol), $\text{C}_5\text{H}_6\text{N}_2$ (2-aminopyridine) (0.10 g, 1.062 mmol) and distilled water (25 ml). The pH of the mixture was necessarily adjusted to 6.5 with $\text{NH}_3\cdot \text{H}_2\text{O}$ solution. The mixture was heated under autogenous pressure at 160 °C for 5 days and then left to cool to room temperature. Dark block crystals could be isolated in about 61% yield (based on Mo). Elemental analyses (%) calcd.: Mo, 44.54; P, 1.20; Cu, 7.38; C, 16.26; H, 1.21; N, 4.34. Found: Mo, 44.48; P, 1.09; Cu, 7.33; C, 16.42; H, 1.19; N, 4.29. FT-IR (KBr, cm^{-1}): 1648, 1616, 1532, 1486, 1414, 1438, 1311, 1221, 1162, 1052, 943, 851, 781, 508, 379.

2.2.3. Preparation of $[\text{Cu}_2(4,4'\text{-bpy})_2][\text{HPMo}_{12}\text{O}_{40}](\text{C}_5\text{H}_6\text{N}_2)$ (3). Compound 3 was synthesized hydrothermally from a mixture of $\text{H}_3\text{Mo}_{12}\text{O}_{40}\cdot \text{P}\cdot \text{xH}_2\text{O}$ (FW \approx 1825.25, 0.5 g, 0.274 mmol), $\text{C}_6\text{H}_5\text{NO}_2$ (2-picolinic acid) (0.16, 1.357 mmol), $\text{CuCl}_2\cdot 2\text{H}_2\text{O}$ (0.333 g, 1.953 mmol), 4,4'-bpy (0.20 g, 1.04 mmol), $\text{C}_5\text{H}_6\text{N}_2$ (2-aminopyridine) (0.10 g, 1.062 mmol) and distilled water (25 ml). The pH of the mixture was necessarily adjusted to 6 with $\text{NH}_3\cdot \text{H}_2\text{O}$ solution. The mixture was heated under autogenous pressure at 160 °C for 5 days and then left to cool to room temperature. Dark block crystals could be isolated in about 58% yield (based on Mo). Elemental analyses (%) calcd.: Mo, 48.85; P, 1.31; Cu, 5.39; C, 12.74; H, 0.98; N, 3.57. Found: Mo, 48.55; P, 1.23; Cu, 5.06; C, 12.94; H, 0.87; N, 3.51. FT-IR (KBr, cm^{-1}): 1653, 1609, 1532, 1481, 1417, 1385, 1321, 1218, 1064, 949, 872, 783, 501, 373.

2.2.4. Preparation of $[\text{Cu}(\text{Phen})(4,4'\text{-bpy})(\text{H}_2\text{O})_2][\text{PW}_{12}\text{O}_{40}](4,4'\text{-bpy})$ (4). Compound 4 was synthesized hydrothermally from a mixture of $\text{Na}_2\text{WO}_4\cdot 2\text{H}_2\text{O}$ (0.5 g, 1.516 mmol), H_3PO_4 (0.20 ml, 85%), $\text{C}_6\text{H}_5\text{NO}_2$ (isonicotinic acid) (0.1 g, 0.812 mmol), $\text{CuCl}_2\cdot 2\text{H}_2\text{O}$ (0.201 g, 1.179 mmol), Phen (0.133 g, 0.671 mmol), 4,4'-bpy (0.052 g, 0.271 mmol) and distilled water (25 ml). The pH of the mixture was necessarily adjusted to 5 with $\text{NH}_3\cdot \text{H}_2\text{O}$ solution. The mixture was heated under autogenous pressure at 160 °C for 5 days and then left to cool to room temperature. Blue block crystals could be isolated in about 45% yield (based on W). Elemental analyses (%) calcd.: W, 57.02; P, 0.80; Cu, 3.28; C, 16.76; H, 1.15; N, 3.62. Found: W, 56.77; P, 0.86; Cu, 3.43; C, 16.58; H, 1.06; N, 3.49. FT-IR (KBr, cm^{-1}): 1602, 1583, 1519, 1493, 1430, 1385, 1378, 1218, 1103, 1064, 955, 885, 808, 712, 514, 366.

2.3. X-ray crystallographic analysis

All the reflection intensity data of compounds 1–4 were collected on a Bruker Apex II diffractometer equipped with graphite monochromated Mo K α (λ = 0.71073) radiation at

room temperature. The structures of compounds 1–4 were solved by direct methods and further refined using the full-matrix least-squares on F^2 using the SHELXTL-97 crystallographic software package. Anisotropic thermal parameters were refined for all the non-hydrogen atoms in compounds 1–4. All hydrogen atoms of ligands were placed in geometrically calculated positions and refined with fixed isotropic displacement parameters using a riding model except the lattice water molecules in compounds 2. A summary of the crystallographic data and structure refinements for compounds 1–4 is given in Table 1. CCDC: 1006424 for 1, 1006425 for 2, 1006426 for 3 and 1006427 for 4.

3. Results and discussion

3.1 Syntheses

$\text{H}_2\text{C}_2\text{O}_4\cdot 2\text{H}_2\text{O}$ plays an important role in the preparation of compound 1 as a reducing agent used to reduce Cu^{2+} to Cu^+ , which has been demonstrated by compounds previously reported by us and other people.¹³

Attempts to synthesize compound 2 without the addition of isophthalic acid or NH_4VO_3 have already been done. Only unidentified amorphous powders were obtained. The roles of NH_4VO_3 and isophthalic acid are still elusive.

The role of 2-picolinic acid for the preparation of compound 3 and the role of isonicotinic acid for the preparation of compound 4 are both still elusive. Firstly we think isophthalic acid for compound 2, 2-picolinic acid for compound 3 and isonicotinic acid for compound 4 perhaps play identical roles to that of $\text{H}_2\text{C}_2\text{O}_4\cdot 2\text{H}_2\text{O}$ for compound 1, all acting as reducing agents to reduce Cu^{2+} to Cu^+ . However, the synthesis of compound 4 containing Cu^{2+} ions demonstrated that this speculation is not right. Therefore, the roles of these different acids except $\text{H}_2\text{C}_2\text{O}_4\cdot 2\text{H}_2\text{O}$ are still elusive.

3.2. Structure descriptions

3.2.1. Crystal structure of compound 1. Single crystal X-ray diffraction analysis reveals that the asymmetric unit of compound 1 consists of half a pseudo-Keggin anion $[\text{HSiW}_{12}\text{O}_{40}]^{3-}$, one and a half $[\text{Cu}(4,4'\text{-bpy})]_3^{3+}$ TMC and half a dissociated imidazole moiety. $[\text{HSiW}_{12}\text{O}_{40}]^{3-}$ contains a disordered $[\text{SiO}_4]^{4-}$ tetrahedron at its center with Si surrounded by eight half-occupied oxygens. Si–O distances are in the range of 1.49(3)–1.70(2) Å. According to different coordination environments, W–O bonds can be classified into three sets: W–O_t (terminal oxygens) with distances of 1.64(2)–1.70(2) Å, W–O_b (bridging oxygens) with distances of 1.84(2)–1.96(3) Å and W–O_c (central oxygens) with distances of 2.29(2)–2.40(2) Å. The oxidation states of W and Cu were calculated using the parameters given by Brown.¹³ The results give the average values 6.0 for tungsten and 0.9 for copper, which reveal that tungsten and copper are in +6 and +1 oxidation states.

There exist two different 1-D $[\text{Cu}(4,4'\text{-bpy})]_n^{n+}$ linear chains in compound 1. The first is constructed from Cu(1) and N(1) 4,4'-bpy. As shown in Fig. 1, Cu(1) is coordinated by two nitrogens from two 4,4'-bpy with Cu–N distances of 1.87(2)–1.91(2) Å

Table 1 Crystal data and structural refinements for compounds 1–4

	Compound 1	Compound 2	Compound 3	Compound 4
Empirical formula	C ₃₃ H ₂₉ Cu ₃ N ₈ O ₄₀ SiW ₁₂	C ₃₅ H ₃₁ Cu ₃ Mo ₁₂ N ₈ O _{40.5} P	C ₂₅ H ₂₃ Cu ₂ Mo ₁₂ N ₆ O ₄₀ P	C ₅₄ H ₄₄ Cu ₂ N ₁₀ O ₄₂ PW ₁₂
Formula weight	3602.46	2584.55	2356.84	3869.14
Crystal system	Triclinic	Monoclinic	Monoclinic	Monoclinic
space group	$\bar{P}1$	<i>C2/c</i>	<i>P2(1)/c</i>	<i>C2/m</i>
<i>a</i> (Å)	10.882(2)	23.402(2)	10.8252(14)	22.726(4)
<i>b</i> (Å)	11.587(2)	21.760(2)	10.8613(14)	15.455(3)
<i>c</i> (Å)	13.273(3)	26.461(3)	23.243(3)	12.036(2)
α (°)	113.30(3)	90.00	90.00	90.00
β (°)	96.32(3)	116.239(2)	104.379(5)	115.17(3)
γ (°)	95.46(3)	90.00	90.00	90.00
Volume (Å ³)	1510.0(5)	12 086(2)	2647.2(6)	3826.0(12)
<i>Z</i>	1	8	2	2
<i>D_C</i> (Mg m ⁻³)	3.962	2.841	2.957	3.359
μ (mm ⁻¹)	23.901	3.564	3.663	18.619
<i>F</i> (000)	1591	9816	2223	3469
θ for data collection	3.05 to 27.48	1.81 to 28.37	1.94 to 28.41	3.06 to 27.48
Reflections collected	14 690	39 475	16 947	18 862
Unique reflections	6788	14 849	6590	4515
<i>R</i> (int)	0.0793	0.0469	0.0394	0.0523
Completeness to θ	98.0	98.1	98.8	99.0
Parameters	473	896	427	277
GOF on <i>F</i> ²	1.064	1.026	1.015	1.027
<i>R</i> ^a [<i>I</i> > 2 σ (<i>I</i>)]	<i>R</i> ₁ = 0.0688	<i>R</i> ₁ = 0.0549	<i>R</i> ₁ = 0.0566	<i>R</i> ₁ = 0.1017
<i>R</i> ^b (all data)	w <i>R</i> ₂ = 0.1758	w <i>R</i> ₂ = 0.1555	w <i>R</i> ₂ = 0.1454	w <i>R</i> ₂ = 0.2347

$$^a R_1 = \sum ||F_o| - |F_c|| / \sum |F_o|, \quad ^b wR_2 = \{ \sum [w(F_o^2 - F_c^2)^2] / \sum [w(F_o^2)^2] \}^{1/2}.$$

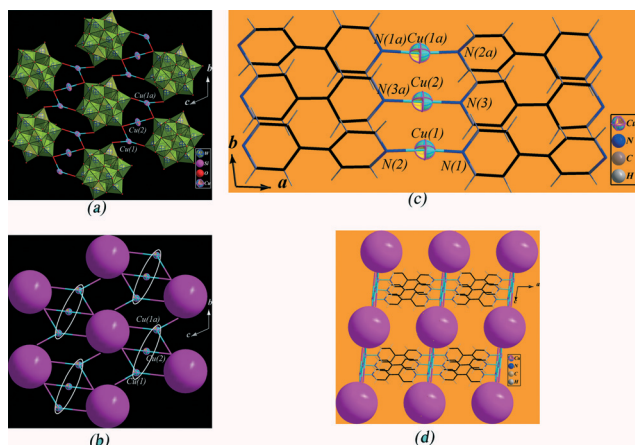


Fig. 1 (a) Ball-and-stick and polyhedral representation of the layer formed by POMs and metal ions; (b) schematic representation of the layer formed by POMs and metal ions; (c) triple-stranded linear chain in compound 1; (d) 3-D structure of compound 1. Symmetry code: a, 1 - *x*, 1 - *y*, -*z*.

and a N–Cu–N angle of 174.6(8)°. It should be noted that each 4,4'-bpy in the first chain serving as an organic bridge coordinates to two Cu(1) to form an infinite chain structure with the –Cu(1)–bpy–Cu(1)–bpy– linking fashion. The second chain is almost identical to the first, which is formed by Cu(2) and N(3) 4,4'-bpy. Cu(2) and N(3) 4,4'-bpy in the second play the same roles as Cu(1) and N(1) 4,4'-bpy in the first.

Cu(1) and Cu(2) chains both contain *n*+ positive charge; however, the two are not as far away from each other, but are arranged near each other with a Cu–Cu distance of 3.6630(8) Å. The reason comes from the strong $\pi \cdots \pi$ interactions

between 4,4'-bpy ligands in two neighboring chains. As shown in Fig. 1, the N(1) and N(2) pyridine rings of each N(1) 4,4'-bpy of the Cu(1) chain are almost coplanar; whereas the two N(3) pyridine rings of each N(3) 4,4'-bpy of the Cu(2) chain are noncoplanar and are twisted with a dihedral angle of 23.581°. The dihedral angle between the N(1) ring in the Cu(1) chain and the neighboring N(3) ring in the Cu(2) chain is also about 0°, meaning that the N(1) ring in the Cu(1) chain is parallel to the N(3) ring in the neighboring Cu(2) chain. Further investigation also found that the plane to plane or centroid to centroid distance of the N(1) and N(3) rings from two neighboring chains is about 3.30 Å, which means that strong $\pi \cdots \pi$ interactions exist. It should be noted that there are two Cu(1) chains sandwiching a Cu(2) chain to form a triple-stranded linear chain structure.

Detailed analysis reveals that copper ions in the abovementioned chains show weak interactions with neighboring POMs, as shown in Fig. 1. Cu(1) receives contributions not only from two nitrogens belonging to two 4,4'-bpy ligands but also from three terminal oxygens belonging to three neighboring POMs with Cu–O distances of 2.790(1)–2.8437(9) Å, exhibiting a trigonal bipyramidal coordination environment (Fig. S1†). In contrast, Cu(2) is actually four-coordinated not only by two nitrogens from two 4,4'-bpy but also by two terminal oxygens from two neighboring POMs with a Cu–O distance of 2.8408(7) Å, displaying a square planar geometry (Fig. S1†). Thus, Cu(1) and Cu(2) act as two bridges interconnecting POMs to form a novel 2-D layered framework structure through weak Cu–O interactions. That is to say, Cu(1) and Cu(2) acting as a μ_3 bridge and a μ_2 bridge, respectively, link three and two neighboring POMs *via* interactions between copper ions and

their neighboring POM terminal oxygens. It should be noted that these Cu–O interactions observed in compound 1 are very weak, thus the coordination spheres about Cu(1) and Cu(2) are only pseudo-trigonal-bipyramidal and pseudo-square-planar geometries (Fig. S1†). One of the most striking features of the 2-D layered framework structure formed by copper ions and POMs is that the layer is perpendicular to the triple-stranded linear chains; that is to say, the layer is also perpendicular to the Cu(1) and Cu(2) chains.

Each POM in compound 1 does not act as a terminal ligand but as a bridging ligand. As shown in Fig. 1, each POM not only coordinates to six Cu(1) in six Cu(1) chains, but also simultaneously coordinates to two Cu(2) in two Cu(2) chains. Thus, each POM acts as a node interconnecting eight adjacent copper chains forming a novel 3-D framework structure. Alternatively, each POM links four tri-stranded linear chains. Through the linkage between Cu ions of chains and oxygens of POMs, $[\text{Cu}(4,4'\text{-bpy})]_n^{n+}$ chains are connected to form a novel 3-D framework structure. It should be noted that the framework is constructed from copper ions, 4, 4'-bpy ligands and POMs connected together in a POM–M–L–M–POM linking fashion, thus, it is a POMMOF.

Except for the POMMOF, there are dissociated imidazoles filling the void space of the POMMOF framework. It should be noted that previously reported POMMOFs did not contain organic moieties as space filling species. The imidazole is disorderedly distributed over two positions. The space filling imidazoles can be removed without the decomposition of compound 1.

3.2.2. Crystal structure of compound 2. It is very interesting to compare the structures of compounds 1 and 2. Compound 1 crystallizes in the triclinic space group $\bar{P}1$, whereas compound 2 crystallizes in the monoclinic space group $C2/c$. The cell parameters of compound 1 are 10.882(2) Å, 11.587(2) Å, 13.273(3) Å, 113.30(3)°, 96.32(3)°, 95.46(3)°, and those of compound 2 are 23.402(2) Å, 21.760(2) Å, 26.461(3) Å, 90.000°, 116.239(2)°, 90.000°. The cell parameters and crystal systems suggested that compound 2 should be thoroughly different from compound 1. However, the X-ray crystallographic study reveals that the packing structures of the two compounds are almost identical to each other.

The asymmetric unit of compound 2 consists of a Keggin anion $[\text{PMo}_{12}\text{O}_{40}]^{3-}$, a $[\text{Cu}(4,4'\text{-bpy})]_{2.5}^{2.5+}$, a dissociative 2-aminopyridine and half a water molecule. The first difference between compound 1 and 2 is the cluster anion, it is a pseudo-Keggin anion $[\text{HSiW}_{12}\text{O}_{40}]^{3-}$ in compound 1 but a Keggin anion $[\text{PMo}_{12}\text{O}_{40}]^{3-}$ in compound 2. The second difference between the two is that compound 2 contains an extra 2-aminopyridine, but compound 1 contains an extra imidazole. Bond valence sum (BVS) calculations for molybdenum and copper atoms in compound 2 reveal that molybdenum atoms are in the +6 oxidation state and copper atoms are in the +1 oxidation state.¹³

There also exist two different 1-D $[\text{Cu}(4,4'\text{-bpy})]_n^{n+}$ linear chains in compound 2. One chain is similar to that in compound 1, which is constructed from copper ions linked

by 4,4'-bpy bridges to a 1-D chain with a $-\text{Cu}(2)\text{-bpy-Cu}(2)\text{-bpy-}$ linking fashion. However, the other chain in compound 2 is thoroughly different from that of compound 1, which contains two crystallographically independent copper ions (Cu(1) and Cu(3)) and two crystallographically independent 4,4'-bpy ligands (N(1) and N(3) 4,4'-bpy) in it. Each 4,4'-bpy in the chain serves as an organic bridge interconnecting two different copper ions to form a novel infinite chain structure with the $-\text{Cu}(1)\text{-bpy-Cu}(3)\text{-bpy-}$ linking fashion which is different from that in compound 1. Therefore, compound 2 also contains two different $[\text{Cu}(4,4'\text{-bpy})]_n^{n+}$ chains.

Compound 1 contains novel triple-stranded linear chains. Compound 2 contains similar triple-stranded linear chains too. However, the further investigation found that the two triple-stranded chains are thoroughly different. The dihedral angle between the two pyridine rings (N(5) and N(6) rings) of each 4,4'-bpy in the Cu(2) chain is 16.170°, and the dihedral angles between the two pyridine rings (N(1), N(2) rings and N(3), N(4) rings) of the two independent 4,4'-bpy in the Cu(1)–Cu(3) chains are 25.246° and 37.136°, respectively. It should be noted that pyridine rings are not only parallel to each other in each 4,4'-bpy but also not parallel to any neighboring pyridine rings of 4,4'-bpy in neighboring chains. That is to say, there exist no $\pi\cdots\pi$ interactions between any two neighboring chains. Therefore, the Cu–Cu distance of two neighboring chains is 3.8511(3)–3.8895(3) Å, which is longer than that in compound 1. And the triple-stranded linear chains in compound 2 are not mainly directed by $\pi\cdots\pi$ interactions.

Copper ions in chains also show weak interactions with neighboring POMs, as shown in Fig. 2. Cu(1) displays a seesaw geometry (which is different from those around both independent copper atoms in compound 1) by being bonded not only to two nitrogens from two 4,4'-bpy but also to two

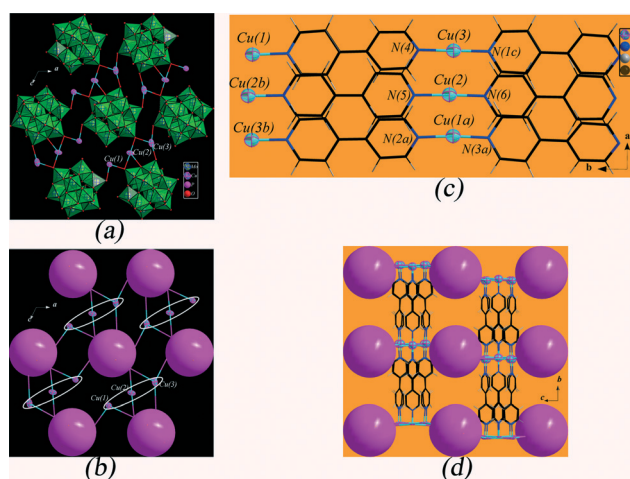


Fig. 2 (a) Ball-and-stick and polyhedral representation of the layer formed by POMs and metal ions in compound 2; (b) schematic representation of the layer formed by POMs and metal ions; (c) triple-stranded linear chain in compound 2; (d) 3-D structure of compound 2. Symmetry codes: a, $-0.5 - x, -0.5 + y, 0.5 - z$; b, $-0.5 - x, 0.5 + y, 0.5 - z$; c, $x, -1 + y, z$.

terminal oxygens from two neighboring POMs with Cu–O distances of 2.7532(3) Å and 2.5850(2) Å (Fig. S2†). Cu(2) is bonded not only to two nitrogens from two 4,4'-bpy but also to three oxygens from three neighboring POM anions, which is identical to Cu(1) in compound 1. However, detailed analysis found that two of the three oxygens are terminal ones with Cu–O distances of 2.7931(3) Å and 2.6650(3) Å, and the remaining one is a bridging oxygen with a Cu–O bond distance of 2.8730(2) Å, thus Cu(2) exhibits a trigonal bipyramidal coordination environment which is different from that around Cu(1) in compound 1 (Fig. S2†). Cu(3) is five-coordinated, its two coordination sites are occupied by two nitrogens from two 4,4'-bpy ligands, and the other three sites are occupied by three terminal oxygens from three neighboring POMs with Cu–O distances of 2.8051(2)–2.8382(2) Å, exhibiting a trigonal bipyramidal geometry, which is similar to that around Cu(1) in compound 1 (Fig. S2†). Further investigation of the three copper coordination spheres found that two coordination oxygens in the coordination sphere of Cu(2) is from one POM, thus Cu(2) and Cu(3), both of which are similar to those corresponding ones Cu(2) and Cu(1a) in compound 1, act as a μ_2 bridge linking two POMs and a μ_3 bridge linking three POMs, respectively. Cu(1), which is different from its corresponding one (Cu(1)) in compound 1, only acts as a μ_2 bridge linking two POMs. Cu(1), Cu(2) and Cu(3) link neighboring POMs to form a novel 2-D layered framework structure which exhibits an almost identical packing motif to that of compound 1. Also the 2-D layer is perpendicular to the triple-stranded linear chains in compound 2. It should be noted that the Cu–O interactions observed in compound 2 are very weak too, the coordination spheres about Cu(1), Cu(2) and Cu(3) are only pseudo-seesaw, pseudo-trigonal-bipyramidal and pseudo-trigonal-bipyramidal geometries (Fig. S2†). However, these Cu–O interactions are relatively stronger than those observed in compound 1, indicating that the framework of compound 2 is relatively stable than that of compound 1.

As shown in Fig. 2, each POM acts as a node interconnecting seven adjacent $[\text{Cu}(4,4'\text{-bpy})_n]^{n+}$ chains to form a novel 3-D framework structure, which is only slightly different from that in compound 1. Alternatively, each POM links four triple-stranded linear chains. Through the linkages between Cu ions of chains and oxygens of POMs, $[\text{Cu}(4,4'\text{-bpy})_n]^{n+}$ chains are connected to form a novel 3-D POMMOF framework structure, which is identical to that of compound 1.

Though the cell parameters and crystal space groups of compounds 1 and 2 are thoroughly different, the packing structures of the two are very similar. It should be noted that the dissociated imidazole and 2-aminopyridine ligands have almost no influence on the packing structures of the two, both of which only play the role of space-filling agents.

3.2.3. Crystal structure of compound 3. Single crystal X-ray diffraction analysis reveals that the asymmetric unit of compound 3 consists of a pseudo-Keggin anion $[\text{HPMo}_{12}\text{O}_{40}]^{2-}$, a $[\text{Cu}(4,4'\text{-bpy})_2]^{2+}$ and a dissociative 2-aminopyridine. Bond valence sum (BVS) calculations for molybdenum and copper

atoms reveal that the oxidation state of molybdenum is +6 and the oxidation state of copper is +1.¹³

There also exists a similar $[\text{Cu}(4,4'\text{-bpy})_n]^{n+}$ linear chain in compound 3 to those in compounds 1 and 2. As shown in Fig. 3, Cu(1) is coordinated by two nitrogens from two different 4,4'-bpy ligands with a Cu–N distance of 1.897(6) Å and a N–Cu–N angle of 177.0(4)° to form a $[\text{Cu}(4,4'\text{-bpy})_n]^{n+}$ chain with a $-\text{Cu}(1)\text{-bpy-Cu}(1)\text{-bpy}-$ linking fashion. However, the chain in compound 3 is only a single-stranded chain which does not form a triple-stranded linear chain.

Detailed analysis reveals that copper ions in the chain show interactions with POMs, as shown in Fig. 3. Cu(1) receives contributions not only from two nitrogens of two 4,4'-bpy but also from two oxygens from one POM with Cu–O distances of 2.7318(97) and 2.8036(3) Å, exhibiting a seesaw geometry. On the other hand, each POM acts as a bridging ligand coordinating to two copper ions in the two neighboring chains to form a novel 1-D ladder-like structure, as shown in Fig. 3, in which $[\text{HPMo}_{12}\text{O}_{40}]^{2-}$ clusters act as ladder rungs, and $[\text{Cu}(4,4'\text{-bpy})_n]^{n+}$ chains act as edges of the ladder. Thus POMs, copper ions and 4,4'-bpy ligands construct a novel 1-D POMMOF.

The 1-D POMMOF chain is further connected to its neighboring chain by O–H...O interactions to form a novel 2-D supramolecular framework structure, as shown in Fig. 3. The oxygen–oxygen distance of the O–H...O interaction is 2.8598(3) Å, which is in the range of general hydrogen bonding interaction. However, the hydrogen atom between the two oxygens of the O–H...O interaction cannot be located by X-ray diffraction analysis. The disordered 2-aminopyridines act as space fillers, which show weak interactions with neighboring 1-D POMMOFs. The shortened distance of disordered nitrogens of 2-aminopyridine and POM oxygens is 2.8646(3) Å.

It should be noted that we have already reported a similar compound to compound 3 very recently.¹⁴ The comparison of the two compounds is also very interesting. Compound 3

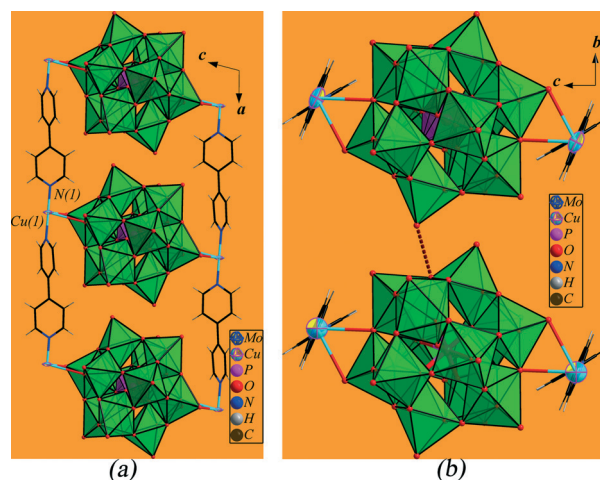


Fig. 3 (a) Ball-and-stick and polyhedral representation of the chain formed by POMs, metal ions and organic ligands in compound 3; (b) ball-and-stick and polyhedral representation of the interaction between two neighboring chains in compound 3.

crystallizes in the monoclinic space group $P2(1)/c$ with cell parameters of 10.8252(14) Å, 10.8613(14) Å, 23.243(3) Å, 90.00°, 104.379(5)°, 90.00°, and the reported compound crystallizes in the triclinic space group $\bar{P}1$ with cell parameters of 10.8645(9) Å, 11.817(1) Å, 13.318(1) Å, 105.386(6)°, 102.406(5)°, 115.660(4)°. ¹⁴ The relationship between compound 3 and the recently reported one ¹⁴ is very similar to that of compounds 1 and 2. Though the cell parameters of the two are thoroughly different, the packing structures of the two are almost identical. Also, compound 3 is based on pseudo-Keggin clusters and the reported compound is based on Keggin anions.

Discussion: why the two compounds with almost identical packing structures crystallize in different crystal space groups with different cell parameters.

Then here we want to know why the two compounds with almost identical packing structures crystallize in different crystal space groups with different cell parameters. We think it should arise from the different POMs or different dissociated organic ligands, but which one should be the main reason?

It is well known that Keggin ions exhibit T_d symmetry. As shown in Fig. 4(b), the twelve molybdenums in the Keggin ion of compound 2 can be divided into four trimers, the metal–metal distances in each trimer are in the range of 3.41–3.44 Å, while the metal–metal distances between neighboring metals from different trimers are in the range of 3.67–3.69 Å. Therefore, the Keggin ion exhibits T_d symmetry. However, the pseudo-Keggin ion is different, not only the center XO_4 tetrahedron becomes a distorted cubic, but also the shell tetrahedron becomes an almost distorted cubic too. As shown in Fig. 4(a), the twelve tungstens in the pseudo-Keggin ion of compound 1 can be divided into two sets of four-trimers, one is represented as red, and the other is represented as green. It should be noted that the metal–metal distances of each red triangle are comparable to the corresponding metal–metal distances of each green triangle, indicating that all the metal–metal distances of the pseudo-Keggin ion are almost identical. Thus the pseudo-Keggin ion exhibits a higher symmetry than the Keggin one, which is near O_h symmetry. Therefore, compound 1 (pseudo-Keggin) crystallizes in a smaller cell and compound 2 (Keggin) crystallizes in a bigger cell.

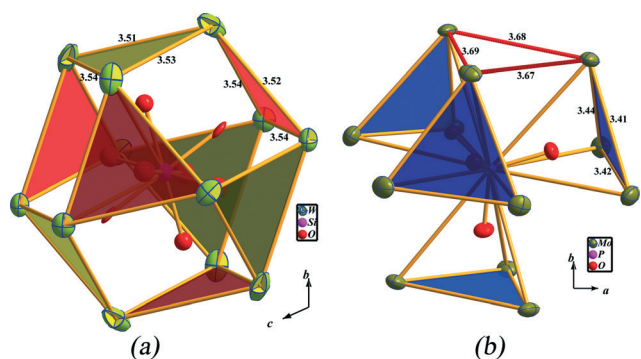


Fig. 4 Difference between pseudo-Keggin (a) and Keggin (b) ions.

When will the structure be based on pseudo-Keggin or Keggin? The heteroatom of the cluster of compound 1 (pseudo-Keggin) is Si, whereas that of the cluster of compound 2 (Keggin) is P. Will the heteroatoms influence the formation of Keggin and pseudo-Keggin ions? The relationship between compound 1 (pseudo-Keggin) and 2 (Keggin) is reminiscent of the relationship between compound 3 and the compound reported by us very recently as mentioned above. ¹⁴ The heteroatom of the cluster of compound 3 (pseudo-Keggin) is P, whereas the heteroatom of the cluster of the reported compound (Keggin) is Si. ¹⁴ Therefore, the heteroatom is not the main reason for the formation of Keggin and pseudo-Keggin ions.

Liu *et al.* also synthesized a compound with the formula $(4,4'\text{-H}_2\text{bpy})\{\text{Cu}(4,4'\text{-bpy})_2[\text{SiW}_{12}\text{O}_{40}]\}$ (ref. 15), which is isomorphous and isostructural to the compound (Keggin) reported by us recently, ¹⁴ but the POM of Liu's compound is a tungsten-based pseudo-Keggin ion. The relationship between Liu's compound (pseudo-Keggin) ¹⁵ and the compound (Keggin) reported by us recently ¹⁴ demonstrated that the difference between Keggin and pseudo-Keggin ions will not surely lead to the difference in the final packing structures.

The dissociated organic ligand in compound 1 is imidazole and that in compound 2 is 2-aminopyridine. It should be noted that the packing structures of compounds 1 and 2 are identical but the dissociated organic ligands and the Keggin ion conformations of the two are different. We think perhaps that the different organic moieties in compounds 1 and 2 are the main reason which makes the two exhibit almost identical packing structures but crystallize in different crystal space groups with different cell parameters, and also makes the POMs in compounds 1 and 2 exhibit different Keggin ion conformations: pseudo-Keggin and Keggin ions.

3.2.4. Crystal structure of compound 4. The asymmetric unit of compound 4 is constructed from a pseudo-Keggin polyoxoanion $[\text{PW}_{12}\text{O}_{40}]^{4-}$, two $[\text{Cu}(\text{Phen})(4,4'\text{-bpy})(\text{H}_2\text{O})]^{2+}$ and a dissociative 4,4'-bpy. Bond valence sum (BVS) calculations reveal that the formula of $\{\text{PW}_{12}\text{O}_{40}\}$ is $[\text{PW}_{11}^{\text{VI}}\text{W}^{\text{V}}\text{O}_{40}]^{4-}$. ¹³

Different from the first three compounds, compound 4 contains a novel 1-D $[\text{Cu}(\text{Phen})(4,4'\text{-bpy})(\text{H}_2\text{O})]_{2n}^{4n+}$ infinite zigzag chain transition metal complex, which is constructed from copper ions and two different organic ligands. As shown in Fig. 5, Cu(1) is coordinated by two N(1) and two N(2) atoms from two different 4,4'-bpy and a Phen ligand with Cu–N distances of 2.025(11)–2.029(11) Å and N–Cu–N angles of 79.9(11)–87.1(10)° and an oxygen atom from a water molecule with a Cu–O distance of 2.29(3) Å. On the other hand, each Phen coordinates to a copper ion as a chelating ligand to form a Cu(phen) TMC, and then each 4,4'-bpy ligand serves as an organic bridge joining two Cu(phen) to form a novel 1-D zigzag chain structure with a $-\text{Cu}(1)\text{-bpy-Cu}(1)\text{-bpy}-$ linking fashion. Therefore, the 1-D chain in compound 4 is different from those in compounds 1–3, the chains in compounds 1–3 are all straight chains, whereas the chain in compound 4 is a zigzag one. The second difference is that the chain in compounds 1–3 are all based on only one type of organic ligand, whereas the chain in compound 4 is based on two

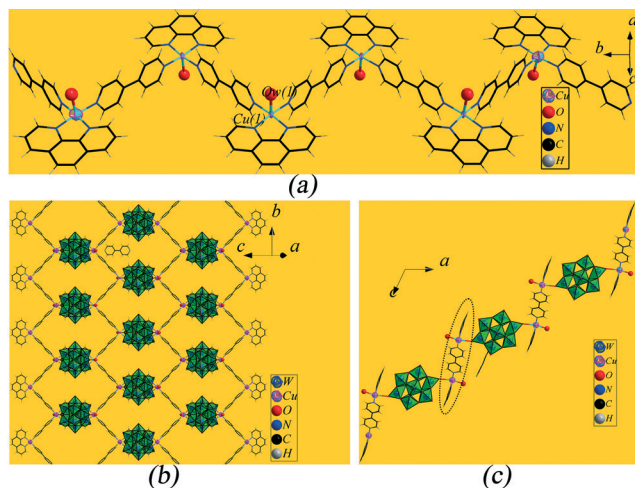


Fig. 5 (a) 1-D transition metal chain complex in compound 4. (b) Upper-view of the 2-D POMMOF framework structure in compound 4. (c) Side-view of the 2-D POMMOF framework structure in compound 4.

different types of organic ligands. The third difference is that the chain in compounds 1–3 are all based on Cu^+ ions, whereas the chain in compound 4 is formed by Cu^{2+} ions. It should be noted that such infinite metal mixed organic complexes are seldom reported previously.

Each copper in the chains shows interactions with neighboring POMs, as shown in Fig. 5. $\text{Cu}(1)$ exhibits a distorted octahedral geometry with four nitrogens (two $\text{N}(1)$ and two $\text{N}(2)$) from two different 4,4'-bpy and a Phen ligand forming the equatorial plane and two oxygens from a water molecule and a neighboring POM with a $\text{Cu}-\text{O}$ distance of 2.63(2) Å occupying the apical positions. Bond valence sums (BVS) calculations for copper atoms reveal that the oxidation state of copper is +2.¹³ On the other hand, as shown in Fig. 5, each POM coordinates to two $\text{Cu}(1)$ ions in two neighboring zigzag chains. Thus, each POM as a bridge interconnects neighboring 1-D zigzag chains to form an unprecedented 2-D sinusoidal layered framework structure. Alternatively, through the linkage between Cu of chains and oxygens of POMs, $[\text{Cu}(\text{Phen})(4,4'\text{-bpy})(\text{H}_2\text{O})]_{2n}^{4n+}$ chains are connected by POMs to form a novel 2-D POMMOF with channels $24.2493(564) \times 5.0074$ Å. To the best of our knowledge, compound 4 is the first example of a POMMOF constructed from POMs, metal ions and mixed organic ligands.

We have synthesized a novel compound $[\text{PMo}_{12}\text{V}_2\text{O}_{42}][\text{Cu}_2(4,4'\text{-bpy})_2][\text{Cu}_2(\text{Phen})(4,4'\text{-bpy})_2] \cdot 3\text{H}_2\text{O}$ very recently, which also contains a novel infinite 1-D zigzag chain transition metal complex which is also constructed from copper ions and two different organic ligands.¹⁶ However, the two 1-D zigzag chains are different from each other, the first one in compound 4 contains a 4,4'-bpy as a bridging ligand joining two neighboring $[\text{Cu}(\text{Phen})]^{2+}$, however, the second one in the previously reported compound $[\text{PMo}_{12}\text{V}_2\text{O}_{42}][\text{Cu}_2(4,4'\text{-bpy})_2][\text{Cu}_2(\text{Phen})(4,4'\text{-bpy})_2] \cdot 3\text{H}_2\text{O}$ contains a $[4,4'\text{-bpy}-\text{Cu}-4,4'\text{-bpy}]^+$ unit as a bridge joining two neighboring $[\text{Cu}(\text{Phen})]^+$. Another difference is that the 1-D metal mixed organic complex in

compound 4 is combined with POMs to form a POMMOF; however, the 1-D metal mixed organic complex in the reported compound did not interact with any POMs at all.

It is noteworthy that there exist $\text{N}-\text{H} \cdots \text{O}$ hydrogen bonding interactions between nitrogens from dissociative 4,4'-bpy moieties and oxygens from water molecules. Through $\text{O}-\text{H} \cdots \text{N}$ interactions between oxygens of water molecules and nitrogens of dissociative 4,4'-bpy ligands with a $\text{N}(3) \cdots \text{OW}1$ ($-1-x, 1+y, 1-z$) distance of 2.9400(1067) Å and a $\text{N}(3) \cdots \text{OW}1$ ($x, 1+y, -1+z$) distance of 3.0239(679) Å, 2-D layers connect to each other to generate an interesting 3-D supramolecular network structure.

3.3. Properties

3.3.1. IR spectra. In the IR spectrum of compound 1 (pseudo-Keggin ion), as shown in Fig. S3(a),† the peak at 967 cm^{-1} is due to $\nu(\text{W}-\text{O}_t)$, the peak at 883 cm^{-1} is due to $\nu(\text{W}-\text{O}_b)$, the peak at 788 is due to $\nu(\text{W}-\text{O}_c)$, and the peak as 919 cm^{-1} is due to $\nu(\text{Si}-\text{O})$. A series of bands in the range of $1611\text{--}1182 \text{ cm}^{-1}$ are characteristic of 4,4'-bpy and imidazole in compound 1.¹⁷ It should be noted that the stretching vibrations of different M–O bonds in compound 1 are observed in the similar spectral regions to those of reported SiW_{12} clusters.¹⁷ Compound 4 (pseudo-Keggin ion) contains an almost identical POM to that of compound 1 with SiO_4 replaced by PO_4 . However, the IR spectrum of compound 4 shows somewhat different from peaks from those of reported PW_{12} clusters (Fig. S3(c))†. The IR spectrum of compound 4 shows peaks at 961, 887, and 809 cm^{-1} associated with $\nu(\text{W}-\text{O}_t)$, $\nu(\text{W}-\text{O}_b)$ and $\nu(\text{W}-\text{O}_c)$, whereas the corresponding peaks related to $\nu(\text{W}-\text{O}_t)$, $\nu(\text{W}-\text{O}_b)$ and $\nu(\text{W}-\text{O}_c)$ of reported PW_{12} clusters are observed at about 990, 890, and 810 cm^{-1} , respectively.¹⁷ Furthermore, the peaks at 1107, 1095 and 1067 cm^{-1} correspond to $\nu(\text{P}-\text{O})$ in compound 4, whereas P–O stretching vibrations of reported PW_{12} clusters were only observed at about 1080 cm^{-1} .¹⁷ Bands in the $1157\text{--}1598 \text{ cm}^{-1}$ region of the IR spectrum of compound 4 are due to vibrations of 2,2'-bpy and 4,4'-bpy in compound 4. Firstly we think that the difference in the IR spectra of compound 4 and the reported PW_{12} clusters comes from the difference between pseudo-Keggin PW_{12} and Keggin PW_{12} species. However, a detailed comparison with the reported pseudo-Keggin PW_{12} found that it is not so, pseudo-Keggin PW_{12} clusters reported by Peng¹⁸ exhibit similar IR spectra to the reported PW_{12} clusters.¹⁷ By detailed analysis of the difference between our pseudo-Keggin PW_{12} and Peng's case, we found that one of the tungstates of our pseudo-Keggin PW_{12} in compound 4 is reduced to W^{V} , perhaps this is the reason. We also found that some similar reduced PW_{12} compounds exhibit similar peaks at 1098 and 1065 cm^{-1} , which should be due to P–O bond vibrations.¹⁹ Thus, we concluded that the difference between pseudo-Keggin and Keggin clusters will not result in the obvious difference in their IR spectra.

Compound 2 (Keggin ion) and compound 3 (pseudo-Keggin ion) contain similar $[\text{PMo}_{12}\text{O}_{40}]^{3-}$ POMs; thus, the IR

spectra of the two are very similar. The characteristic peaks of Mo–O_t bonds for POMs in compounds 2 and 3 appear at 976, 955 cm⁻¹ and 979, 957 cm⁻¹, respectively, the peaks at 867, 851 cm⁻¹ for compound 2 and 875, 853 cm⁻¹ for compound 3 can be attributed to $\nu(\text{Mo}-\text{O}_b-\text{Mo})$. The peak at 788 cm⁻¹ for compound 2 and 791 cm⁻¹ for compound 3 can be attributed to $\nu(\text{Mo}-\text{O}_c-\text{Mo})$.¹⁷ IR spectra exhibit bands at 1073, 1053 cm⁻¹ and 1060 cm⁻¹ characteristic of P–O bonds of PO₄³⁻ groups which were observed in compounds 2 and 3, respectively. The IR spectra of pseudo-Keggin PMo₁₂ and Keggin PMo₁₂ also demonstrated the conclusion mentioned above.

3.3.2 TG analysis. The TG curve of compound 1 (Fig. S4†) decreases until 250 °C with a weight loss of 1.93%, which is consistent with the release of imidazole moieties in compound 1 (calculated: 2.28%). Then the curve decreases again until 797 °C with a weight loss of 13.7%, which is due to the release of 4,4'-bpy ligands in compound 1 (calculated: 13.03%).

As mentioned above, compounds 1 and 2 are very similar to each other with almost identical packing structures. However, the TG curves of the two are thoroughly different. The TG curve of compound 2 decreases until 237 °C with a weight loss of 0.65%, which is ascribed to the release of lattice water molecules in compound 2 (calculated: 0.35%). The TG curve then decreases until 644 °C with a weight loss of 21.43%, which corresponds to the combustion of 4,4'-bpy ligands and dissociated 2-aminopyridine moieties in compound 2 (calculated: 21.77%). Imidazole moieties in compound 1 are easily released from the structure of compound 1 (about 250 °C), however, 2-aminopyridine moieties are relatively hard to release from the structure of compound 2 (higher than 360 °C), indicating that 2-aminopyridine moieties are very stable in the structure of compound 2. The reason is that there are strong interactions between dissociated 2-aminopyridine moieties and the framework of compound 2 and 2-aminopyridine is bigger than imidazole which is not easy to release from the framework. The TG analyses of compounds 1 and 2 are well consistent with the structural results of compounds 1 and 2.

The crystal structure of compound 3 is different from that of compound 1, however, the TG curve of compound 3 is similar to that of compound 1. The TG curve of compound 3 can also be divided into two stages, the first stage is also from room temperature to 250 °C with a weight loss of 2.39%, which is due to the release of 2-aminopyridine moieties (calculated: 3.99%). The second stage is from 250 to 656 °C with a weight loss of 15.30%, which is ascribed to the combustion of 4,4'-bpy ligands in compound 3 (calculated: 13.34%). The whole weight loss of compound 3 is 17.69%, which is well consistent with the calculated result (17.33%). Both compounds 2 and 3 contains 2-aminopyridine moieties, however, 2-aminopyridine moieties in compound 2 are hard to release and the ones in compound 3 are relatively easy to release. The reason is that the structure of compound 2 is a 3-D framework, and 2-aminopyridine moieties fill the framework, therefore, it is hard for 2-aminopyridine moieties to be released before the whole framework structure is decomposed.

The TG curve of compound 4 shows obvious decrease from 315 °C, and then continuously decreases until 693 °C with a weight loss of 22.39%, which is consistent with the release of organic moieties and lattice waters in compound 4 (calculated: 22.46%).

3.3.3. XRD analysis. The powder X-ray diffraction patterns of compounds 1–4 are in good agreement with the simulated XRD patterns (Fig. S5†), confirming the phase purity of compounds 1–4. The differences in reflection intensity are probably due to preferential orientations in the powder samples of compounds 1–4. The XRD patterns of the samples of compounds 1 and 3 obtained after calcination at 220 °C for 2 h and the XRD pattern of the sample of compound 2 obtained after calcination at 240 °C for 2 h are also shown in Fig. S5,† these XRD patterns are also in good agreement with the simulated XRD patterns, indicating that the framework structures of compounds 1–3 can still be retained after calcination.

3.3.4. UV-vis spectroscopy. As shown in Fig. S6,† the UV-vis spectrum of compound 1 displays one wide medium intense absorption peak at about 262 nm assigned to the O → W charge transfer in the polyanion of compound 1. The UV-vis spectrum of compound 4 is similar to that of compound 1, which exhibits one wide medium intense absorption peak at 270 nm attributed to charge transfer band of O → W in the polyanion of compound 3. The UV-vis spectra of compounds 2 and 3 are very similar with bands at about 256 and 257 nm, respectively, which should be ascribed to the charge transfer bands of O → Mo in the polyanion of compounds 2 and 3, respectively. All Keggin ions have charge transfer bands at *ca.* 260 nm,^{1b,20} The visible spectra of compounds 1–4 confirm that the POMs did not change in the DMSO solution. All the four UV-vis spectra exhibit unobvious shoulder peaks at about 300–320 nm which can be attributed to $n \rightarrow \pi^*$ transitions in compounds 1–4.

The solid state UV-vis diffuse reflectance spectra of compounds 1–4 were also recorded. As shown in Fig. S7,† the solid state UV-vis noise spectra of compounds 1–3 are similar, each of which displays a broad peak from about 600 nm to 225 nm which should be ascribed to O → M charge transfers, $n \rightarrow \pi^*$ transitions and d–d transitions in compounds 1–3. Not only the peaks originating from O → M charge transfers and $n \rightarrow \pi^*$ transitions in compounds 1–3 are similar, but also the peaks originating from d–d transitions of the three compounds are similar for similar colours (dark) of compounds 1–3, therefore, the solid state UV-vis spectrum curves of compounds 1–3 are very similar. The solid state UV-vis spectrum of compound 4 is different from those of the other three. As shown in Fig. S7,† the spectrum of compound 4 displays two broad peaks, one is from about 470 nm to 225 nm, the other is from 470 nm to 700 nm. The first peak should be due to the O → M charge transfer and $n \rightarrow \pi^*$ transition in compound 4, whereas the second peak is due to the d–d transition in compound 4 (blue).

Comparisons of the solid state UV-vis spectra with solution state UV-vis spectra of compounds 1–4 reveal that each

solid state UV-vis spectrum is essentially similar to its corresponding solution state UV-vis spectrum. The main difference is that the peaks originating from d–d transitions were not observed in the solution state UV-vis spectra of compounds 1–4. The absence of these d–d transition peaks should be attributed to the too dilute solutions of compounds 1–4.

3.3.5. Fluorescence properties. We have examined the fluorescence properties of DMSO solutions of 4,4'-bpy, phen, 2-aminopyridine and compounds 1–4 at room temperature, as shown in Fig. S8†. The fluorescence spectrum of 4,4'-bpy displays an emission peak at 429 nm ($\lambda_{\text{ex}} = 342$ nm) (Fig. S8†), the fluorescence spectrum of phen displays an emission peak at 431 nm ($\lambda_{\text{ex}} = 357$ nm) (Fig. S8†), and the spectrum of free 2-aminopyridine displays an emission peak at 427 nm ($\lambda_{\text{ex}} = 347$ nm) (Fig. S8†). The fluorescence spectrum of compound 1 exhibits an emission peak at 415 nm ($\lambda_{\text{ex}} = 362$ nm) (Fig. S8†). Because the emission band of 1 is similar to that of free 4,4'-bpy ligands in terms of position and band shape, it should be assigned to intraligand electronic transfers of 4,4'-bpy ligands. The fluorescence spectra of compounds 2 and 3 exhibit similar emission peaks at 426 and 432 nm upon excitation at 363 and 364 nm, respectively (Fig. S8†), both of which can be assigned to intraligand electronic transfers of 4,4'-bpy and 2-aminopyridine ligands. The fluorescence spectrum of compound 4 exhibits an emission peak at 410 nm ($\lambda_{\text{ex}} = 345$ nm) (Fig. S8†). The emission peak in compound 4 is blue shifted relative to those of free 4,4'-bpy ligands and free phen ligands. The blue shift has been regarded as due to the complexation of organic ligands with copper atoms.

We not only examined the fluorescence properties of DMSO solutions of 4,4'-bpy, phen, 2-aminopyridine and compounds 1–4, but also collected the solid state fluorescence spectra of compounds 1–4 (Fig. S9†). The solid state fluorescence spectra of compounds 1–4 display very similar emission peaks at 424 nm ($\lambda_{\text{ex}} = 374$ nm), 423 nm ($\lambda_{\text{ex}} = 373$ nm), 424 nm ($\lambda_{\text{ex}} = 373$ nm) and 424 nm ($\lambda_{\text{ex}} = 375$ nm), respectively (Fig. S9†). The comparisons of the solid state fluorescence spectra with the fluorescence spectra in DMSO solutions reveal that each solid state fluorescence spectrum is essentially similar to its corresponding solution state fluorescence spectrum.

3.3.6. Cyclic voltammetry. The cyclic voltammogram of the DMSO solution of compound 1 in 1 mol L⁻¹ H₂SO₄ at a scan rate of 100 mV s⁻¹ is presented in the potential range of -150 to -650 mV (Fig. S10†). There exist three reversible redox peaks with mean peak potentials ($E_{1/2} = (E_{\text{pa}} + E_{\text{pc}})/2$) at -578, -431, -249 mV for the POM ions in compound 1. The three redox peaks correspond to one two-electron and two consecutive one-electron processes of W in the POM ions of compound 1.²¹ The cyclic voltammogram of the DMSO solution of compound 4 recorded under the same conditions as those of compound 1 is presented in the potential range of 200 to -700 mV (Fig. S10(d)†). There exist three reversible redox peaks with mean peak potentials ($E_{1/2} = (E_{\text{pa}} + E_{\text{pc}})/2$) at -606, -367, -253 mV for the POM ions in compound 4. The three

redox peaks also correspond to one two-electron and two consecutive one-electron processes of W in the POM ions of compound 4.²²

The cyclic voltammogram of the DMSO solution of compound 2 recorded under the same conditions as those of compound 1 is presented in the potential range of 500 to -100 mV (Fig. S10†). There exist three reversible redox peaks with mean peak potentials ($E_{1/2} = (E_{\text{pa}} + E_{\text{pc}})/2$) at -19, 225.5, 352.5 mV for the POM ions in compound 2. The three redox peaks correspond to three two-electron processes of Mo in the POM ions of compound 2.²³ The cyclic voltammogram of the DMSO solution of compound 3 recorded under the same conditions as those of compound 1 is presented in the potential range of 500 to -100 mV (Fig. S10†). There exist three reversible redox peaks with mean peak potentials ($E_{1/2} = (E_{\text{pa}} + E_{\text{pc}})/2$) at -28, 218.5, 335 mV for the POM ions in compound 3. The three redox peaks also correspond to three two-electron processes of Mo in the POM ions of compound 3.²³

The compound 1-modified CPE (1-CPE) was fabricated as follows: 3 mg of graphite powder, 1 μ L of Nujol and 1.5 mg of compound 1 were blended and ground thoroughly in an agate mortar. Then the homogeneous mixture was packed into a poly(tetrafluoroethylene) tube with a 1.5 mm inner diameter, and the tube surface was wiped with paper. Electrical contact was established with a Cu rod through the back of the electrode. In a similar manner, 2-, 3-, and 4-CPEs were made with compounds 2–4. Electrochemical measurements were performed with a CHI 660b electrochemical workstation. A conventional three-electrode system was used with Ag/AgCl as a reference electrode and Pt wire as a counter electrode. Chemically bulk-modified carbon-paste electrodes (CPEs) were used as the working electrodes. CV measurements are carried out in a 1 mol L⁻¹ H₂SO₄ aqueous solution.

The cyclic voltammogram of 1-CPE at a scan rate of 100 mV s⁻¹ in the potential range of +600 to -800 mV is shown in Fig. S11†. There exist three reversible redox peaks with mean peak potentials ($E_{1/2} = (E_{\text{pa}} + E_{\text{pc}})/2$) at -622, -515, -252 mV for compound 1, which should be due to one two-electron and two consecutive one-electron processes of W in compound 1.²¹ The cyclic voltammogram of 4-CPE is similar to that of 1-CPE, which also exhibits three reversible redox peaks with mean peak potentials ($E_{1/2} = (E_{\text{pa}} + E_{\text{pc}})/2$) at -594, -482 and -290 mV.

The cyclic voltammogram of 2-CPE exhibits three reversible redox peaks with mean peak potentials ($E_{1/2} = (E_{\text{pa}} + E_{\text{pc}})/2$) at 22, 200 and 312 mV for compound 2. The cyclic voltammogram of 3-CPE shows three reversible redox peaks with mean peak potentials ($E_{1/2} = (E_{\text{pa}} + E_{\text{pc}})/2$) at 33, 245 and 393 mV.

Comparisons of cyclic voltammograms of CPEs of compounds 1–4 with cyclic voltammograms of DMSO solutions of compounds 1–4 reveal that each cyclic voltammogram of CPEs is essentially similar to its corresponding cyclic voltammogram of DMSO solution.

3.3.7. Photocatalytic properties. In a typical process, 1.39 mmol of compound 1 (5 mg), 2 (3.6 mg), 3 (3.28 mg) or

4 (5.4 mg) was ground for about 10 min with an agate mortar to obtain a fine powder, and then the powder was dispersed in 100 mL of Rhodamine B (RhB) solutions (1.0×10^{-5} mol L⁻¹). The suspension was agitated in an ultrasonic bath for 20 min in the dark and then magnetically stirred in the dark for about 30 min. The suspension was finally exposed to UV irradiation from a 300 W Hg lamp at a distance of about 4–5 cm between the liquid surface and the lamp. The suspension was stirred during irradiation at a stirring rate of about 790–800 rpm. At 30 min intervals, 5 mL of samples was taken out of the beaker, was purified by centrifugation at 10 000 rpm for 5 min, and subsequently analyzed by UV-visible spectroscopy (Fig. 6). The photodegradation process of RhB without any photocatalyst has been studied for comparison, and only 27% RhB was photodegraded after 390 min. Changes in the C_t/C_0 plot of RhB solutions *versus* reaction time are shown in Fig. 6. Compared with RhB without any photocatalyst, the absorption peaks of compounds 1–4 decreased obviously upon irradiation, indicating that these compounds have excellent photocatalytic properties. It also reveals that compounds 1–4 are outstanding photocatalysts for photocatalytic degradation of RhB.

Fig. 6 shows the reaction results of photodegradation of RhB over various catalysts at room temperature. As expected, all the catalysts are active for the photodegradation of RhB. Compound 1 catalyst shows the activity with 53.2% conversion after 390 min. Nevertheless, compound 2 shows a lower activity with 47.7% conversion. Compound 3 catalyst shows the lowest conversion of 35.0% among the four. Compound 4 shows the highest conversion (58.8%) among the four.

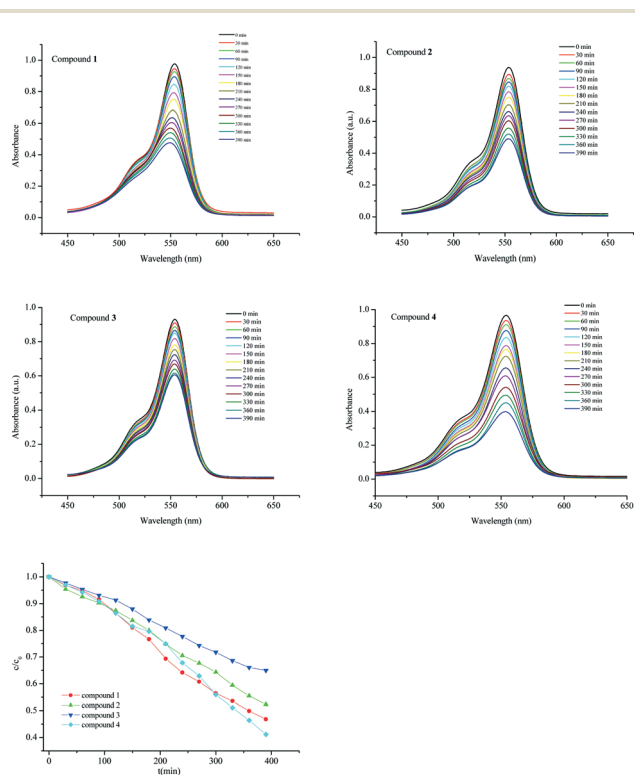


Fig. 6 Photodegradation properties of compounds 1–4.

Both compounds 1 and 2 contain almost identical transition metal ions, organic moieties and have almost identical packing structures, the only significant difference between the two is the Keggin species, it is a tungstate-based Keggin species in compound 1 and a molybdate-based Keggin species in compound 2. The different conversions of RhB perhaps come from the different Keggin species. It is very obvious that the tungstate-based Keggin species will be more active for the photodegradation of RhB than the molybdate-based Keggin species. Such a phenomenon has also been observed by Wang *et al.*²⁴

Compounds 1 and 4 have different packing structures, and the two are based on similar tungstate-based Keggin species, identical transition metal ions, but different organic moieties. The conversion of RhB over compound 4 is slightly higher than that over compound 1. Wang²⁵ and Wang²⁶ have also reported that the conversions of RhB over different compounds even containing identical Keggin species will not be the same.

The photocatalytic reaction occurs in the adsorbed phase (on the surface of the catalyst), and the model of activation of the catalysts is photonic activation by exciting the POM with light energy higher than the band gap of the POM, which leads to an intramolecular charge transfer and the formation of the excited-state species (POM)*.²⁷ The first reason for the different conversions of compounds 1–4 should be the different POMs in them. The second main reason should be perhaps ascribed to the different packing structures of compounds 1–4. The preferential orientations of crystal planes of compounds 1–4 should be different, thus the number of POMs on crystal planes perhaps should be different, and the difference perhaps will lead to their different photocatalytic properties.

Conclusions

In summary, four new compounds based on Keggin polyoxoanions, transition metal ions and organic ligands have been synthesized and characterized. The syntheses of compounds 1–4 confirm that Keggin POMs are powerful building blocks for POMMOF hybrids. Further research is under way to determine the rules of their synthesis and to explore their attractive properties.

Acknowledgements

This work was supported by the National Natural Science Foundation of China, no. 21003056.

Notes and references

- (a) D. L. Long, E. Burkholder and L. Cronin, *Chem. Soc. Rev.*, 2007, 36, 105; (b) M. T. Pope, *Heteropoly and Isopoly Oxometalates*, Springer-Verlag, Berlin, 1983; (c) M. T. Pope and A. Müller, *Angew. Chem., Int. Ed. Engl.*, 1991, 30, 34; (d) M. T. Pope and A. Müller, *Polyoxometalate Chemistry: From Topology via Self-Assembly to Applications*, The Netherlands,

- Kluwer, Dordrecht, 2001; (e) T. Yamase and M. T. Pope, *Polyoxometalate Chemistry for Nano-Composite Design*, The Netherlands, Kluwer, Dordrecht, 2002; (f) A. Proust, B. Matt, R. Villanneau, G. Guillemot and G. L. P. Guozerh, *Chem. Soc. Rev.*, 2012, **41**, 7605; (g) S. Roy, *CrystEngComm*, 2014, **16**, 4667.
- 2 (a) A. Müller and S. Roy, *Coord. Chem. Rev.*, 2003, **245**, 153; (b) A. Müller, P. Kögerler and C. Kuhlmann, *Chem. Commun.*, 1999, 1347–1358.
 - 3 C. L. Hill, *Chem. Rev.*, 1998, **98**, 1.
 - 4 (a) J. W. Han and C. L. Hill, *J. Am. Chem. Soc.*, 2007, **129**, 15094; (b) R. Cao, J. W. Han, T. M. Anderson, D. A. Hillesheim, K. I. Hardcastle, E. Slonkina, B. Hedman, K. O. Hodgson, M. L. Kirk, D. G. Musaev, K. Morokuma, Y. V. Geletii and C. L. Hill, *Adv. Inorg. Chem.*, 2008, **60**, 245.
 - 5 (a) M. I. Khan, E. Yohannes and R. J. Doedens, *Angew. Chem., Int. Ed.*, 1999, **38**, 1292; (b) J. Lu, Y. Xu, N. K. Goh and L. S. Chia, *Chem. Commun.*, 1998, 2733; (c) A. Tripathi, T. Hughbanks and A. Clearfield, *J. Am. Chem. Soc.*, 2003, **125**, 10528; (d) P. J. Hagrman, D. Hagrman and J. Zubieta, *Angew. Chem., Int. Ed.*, 1999, **38**, 2638; (e) S. Reinoso, P. Vitoria, J. M. Gutiérrez-Zorrilla, L. Lezama, L. S. Felices and J. I. Beitia, *Inorg. Chem.*, 2005, **44**, 9731; (f) J. Thomas and A. Ramanan, *Cryst. Growth Des.*, 2008, **8**, 3391.
 - 6 (a) C. Lei, J. G. Mao, Y. Q. Sun and J. L. Song, *Inorg. Chem.*, 2004, **43**, 1964; (b) C. M. Liu, D. Q. Zhang, M. Xiong and D. B. Zhu, *Chem. Commun.*, 2002, 1416; (c) Y. P. Ren, X. J. Kong, X. Y. Hu, M. Sun, L. S. Long, R. B. Huang and L. S. Zheng, *Inorg. Chem.*, 2006, **45**, 4016; (d) G. C. Ou, L. Jiang, X. L. Feng and T. B. Lu, *Dalton Trans.*, 2009, 71; (e) J. Y. Niu, D. J. Guo, J. P. Wang and J. W. Zhao, *Cryst. Growth Des.*, 2004, **4**, 241.
 - 7 (a) X. B. Cui, J. Q. Xu, Y. Li, Y. H. Sun and G. Y. Yang, *Eur. J. Inorg. Chem.*, 2004, 1051; (b) X. B. Cui, J. Q. Xu, H. Meng, S. T. Zheng and G. Y. Yang, *Inorg. Chem.*, 2004, **43**, 8005; (c) C. L. Pan, J. Q. Xu, G. H. Li, X. B. Cui, L. Ye and G. D. Yang, *Dalton Trans.*, 2003, 517; (d) J. W. Zhao, C. M. Wang, J. Zhang, S. T. Zheng and G. Y. Yang, *Chem. – Eur. J.*, 2008, **14**, 9223.
 - 8 (a) H. Y. An, Y. G. Li, E. B. Wang, D. R. Xiao, C. Y. Sun and L. Xu, *Inorg. Chem.*, 2005, **44**, 6062; (b) H. Y. An, Y. G. Li, D. R. Xiao, E. B. Wang and C. Y. Sun, *Cryst. Growth Des.*, 2006, **6**, 1107; (c) C. Y. Sun, Y. G. Li, E. B. Wang, D. R. Xiao, H. Y. An and L. Xu, *Inorg. Chem.*, 2007, **46**, 1563; (d) Y. Lu, Y. Xu, E. B. Wang, X. X. Xu and Y. Ma, *Inorg. Chem.*, 2006, **45**, 2060.
 - 9 (a) B. Z. Lin and S. X. Liu, *Chem. Commun.*, 2002, 2126; (b) L. J. Zhang, X. L. Zhao, J. Q. Xu and T. G. Wang, *J. Chem. Soc., Dalton Trans.*, 2002, 3275.
 - 10 (a) Y. Wang, L. Ye, T. G. Wang, X. B. Cui, S. Y. Shi, G. W. Wang and J. Q. Xu, *Dalton Trans.*, 2010, **39**, 1916; (b) J. Lü, E. H. Shen, Y. G. Li, D. R. Xiao, E. B. Wang and L. Xu, *Cryst. Growth Des.*, 2005, **5**, 65; (c) J. Q. Sha, J. Peng, H. S. Liu, J. Chen, A. X. Tian and P. P. Zhang, *Inorg. Chem.*, 2007, **46**, 11183; (d) A. X. Tian, J. Ying, J. Peng, J. Q. Sha, H. J. Pang, P. P. Zhang, Y. Chen, M. Zhu and Z. M. Su, *Inorg. Chem.*, 2009, **48**, 100; (e) H. Y. An, E. B. Wang, D. R. Xiao, Y. G. Li, Z. M. Su and L. Xu, *Angew. Chem., Int. Ed.*, 2006, **45**, 904.
 - 11 (a) C. Streb, C. Ritchie, D. L. Long, P. Kögerler and L. Cronin, *Angew. Chem., Int. Ed.*, 2007, **46**, 7579; (b) A. Dolbecq, P. Mialane, L. Lisnard, J. Marrot and F. Sécheresse, *Chem. – Eur. J.*, 2003, **9**, 2914; (c) P. Mialane, A. Dolbecq and F. Sécheresse, *Chem. Commun.*, 2006, 3477; (d) B. Nohra, H. E. Moll, L. M. R. Albelo, P. Mialane, J. Marrot, C. Mellot-Draznieks, M. O'Keeffe, R. N. Biboum, J. Lemaire, B. Keita and A. Dolbecq, *J. Am. Chem. Soc.*, 2011, **133**, 13363; (e) S. T. Zheng, J. Zhang and G. Y. Yang, *Angew. Chem., Int. Ed.*, 2008, **47**, 3909.
 - 12 (a) Z. P. Wang, J. H. Yu and R. R. Xu, *Chem. Soc. Rev.*, 2012, **41**, 8210; (b) J. H. Yu and R. R. Xu, *Acc. Chem. Res.*, 2010, **43**, 1195–1204; (c) H. C. Zhou, J. R. Long and O. M. Yaghi, *Chem. Rev.*, 2012, **112**, 673–674; (d) S. B. Choi, H. Furukawa, H. J. Nam, D. Y. Jung, Y. H. Jhon, A. Walton, D. Book, M. O'Keeffe, O. M. Yaghi and J. Kim, *Angew. Chem., Int. Ed.*, 2012, **51**, 8791–8795.
 - 13 I. D. Brown, in *Structure and Bonding in Crystals*, ed. M. O'Keefe and A. Navrotsky, Academic Press, New York, 1981, vol. 2, p. 1.
 - 14 S. Y. Shi, Z. L. Xu, H. H. Teng, L. Z. Zhao, X. B. Cui and J. Q. Xu, *Inorg. Chim. Acta*, 2013, **402**, 123–127.
 - 15 Y. B. Liu, L. M. Wang, L. N. Xiao, Y. Y. Hu, D. C. Zhao, H. Y. Jiang, Y. Peng, X. B. Cui and J. Q. Xu, *J. Coord. Chem.*, DOI: 10.1080/00958972.2014.991919.
 - 16 L. M. Wang, Y. Wang, Y. Fan, L. N. Xiao, Y. Y. Hu, Z. M. Gao, D. F. Zheng, X. B. Cui and J. Q. Xu, *CrystEngComm*, 2014, **16**, 430–440.
 - 17 C. Rocchiccioli-Deltcheff, M. Fournier, R. Franck and R. Thouvenot, *Inorg. Chem.*, 1983, **22**, 207–216.
 - 18 M. G. Liu, P. P. Zhang, J. Peng, H. X. Meng, X. Wang, M. Zhu, D. D. Zhang, C. L. Meng and K. Alimaje, *Cryst. Growth Des.*, 2012, **12**, 1273.
 - 19 L. N. Xiao, Y. Y. Hu, L. M. Wang, Y. Wang, J. N. Xu, H. Ding, X. B. Cui and J. Q. Xu, *CrystEngComm*, 2012, **14**, 8589.
 - 20 O. Glemser and W. Hoeltje, *Z. Naturforsch., B: Anorg. Chem., Org. Chem., Biochem., Biophys., Biol.*, 1965, **20**, 192.
 - 21 S. Q. Liu, Z. Shi and S. J. Dong, *Electroanalysis*, 1998, **10**, 891.
 - 22 M. G. Liu, P. P. Zhang, J. Peng, H. X. Meng, X. Wang, M. Zhu, D. D. Wang, C. L. Meng and K. Alimaje, *Cryst. Growth Des.*, 2012, **12**, 1273.
 - 23 A. X. Tian, J. Ying, J. Peng, J. Q. Sha, Z. M. Su, H. J. Pang, P. P. Zhang, Y. Chen, M. Zhu and Y. Shen, *Cryst. Growth Des.*, 2010, **10**, 1104.
 - 24 A. X. Tian, Y. Yang, J. Ying, N. Li, X. L. Lin, J. W. Zhang and X. L. Wang, *Dalton Trans.*, 2014, **43**, 8405.
 - 25 Q. Lan, J. Zhang, Z. M. Zhang, Y. Lu and E. B. Wang, *Dalton Trans.*, 2013, **42**, 16602.
 - 26 (a) X. L. Wang, D. Zhao, A. X. Tian and J. Ying, *Dalton Trans.*, 2014, **43**, 5211; (b) X. L. Wang, N. Han, H. Y. Lin, A. X. Tian, G. C. Liu and J. W. Zhang, *Dalton Trans.*, 2014, 43.
 - 27 (a) H. Fu, Y. G. Li, Y. Lu, W. L. Chen, Q. Wu, J. X. Meng, X. L. Wang, Z. M. Zhang and E. B. Wang, *Cryst. Growth Des.*, 2011, **11**, 458; (b) D. Y. Chen, A. Sahasrabudhe, P. Wang, A. Dasgupta, R. X. Yuan and S. Roy, *Dalton Trans.*, 2013, **42**, 10587.